Hindawi
Journal of Nanomaterials
Volume 2018, Article ID 4212187, 8 pages
https://doi.org/10.1155/2018/4212187

Research Article

Fabrication of Bifunctional TiO_2/POM Microspheres Using a Layer-by-Layer Method and Photocatalytic Activity for Methyl Orange Degradation

Ping Niu,[1] **Dunqing Wang**,[1] **Aili Wang**,[1] **Yuhua Liang**,[2] **and Xinfang Wang**[1]

[1]*College of Chemistry and Chemical Engineering, Dezhou University, Dezhou 253023, China*
[2]*Department of Dermatology, Dezhou People's Hospital of Shandong Province, Dezhou 253023, China*

Correspondence should be addressed to Ping Niu; np68@sina.com

Received 7 February 2018; Revised 7 May 2018; Accepted 22 May 2018; Published 7 June 2018

Academic Editor: Giuliana Magnacca

Bifunctional films of Keggin-type polyoxometalates $H_3PW_{12}O_{40}$ (PW_{12}), $H_4SiW_{12}O_{40}$ (SiW_{12}), $H_3PMo_{12}O_{40}$ (PMo_{12}), and TiO_2 were successfully built on Fe_3O_4@SiO_2 microspheres using a layer-by-layer method. The characterization by field emission scan electronic microscopy (FESEM) and energy dispersive X-ray spectroscopy (EDX) shows that TiO_2 nanoparticles and polyoxometalate (POM) anions are successfully assembled. The photodegradation of methyl orange (MO) was used to test the photocatalytic efficiency of magnetic catalysts under UV irradiation. For MO decomposition, multilayer films that combine PW_{12} and SiW_{12} with TiO_2 show high efficiency, which can be attributed to the synergistic effect between POMs and TiO_2. The degradation of the model contaminant was also systematically checked under different conditions such as bilayer number deposited on magnetic microspheres, catalyst concentration, inorganic oxidants, and salts. The oxidation process of MO follows an apparent first-order reaction. Furthermore, the composite catalysts deposited on Fe_3O_4@SiO_2 magnetic microspheres can be conveniently, quickly, and efficiently separated by an external magnet from a solution.

1. Introduction

The production and use of synthetic dyes contribute to a massive pollution problem as a result of their high toxicity, slow biodegradation, and potential carcinogenicity [1]. To solve environmental problems caused by dye pollutants, various advanced methods have been adopted. Among these methods, photocatalytic oxidization technology has attracted growing interest on account of its energy saving, highly efficient, nonselective, and environmentally friendly characteristics. Its origin can date back to the 70s of the previous century in the field of wastewater treatment [2]. During the past decades, the nanostructured TiO_2 photocatalyst aroused much interest [3]. However, the fast recombination of photogenerated electrons and holes results in a decrease of photocatalytic efficiency and restricts the practical application of TiO_2.

In contrast to TiO_2, polyoxometalates (POMs) are often used as homogeneous photocatalysts in recent years [4, 5]. POMs are easily soluble in water and difficult to recycle from the reaction system for reuse. In order to overcome these shortcomings, heterogeneous catalysts containing POMs have been prepared by immobilizing POMs on solid supports such as functional microspheres [6–8], indium-tin oxide (ITO) [9], glassy carbon electrode [9, 10], and quartz slides [9, 11].

In recent years, significant attention was focused on the functional thin films containing POMs prepared by a layer-by-layer (LbL) self-assembly method. These films have potential applications in the fields of photoelectrochemistry [12, 13], photocatalysis [7, 14–16], electrocatalysis [17, 18], photochromism [18], sensors [9, 19], and electrochromism [18, 20]. Compared with films assembled by single building blocks, composite films are employed for high performance. Sun et al. [12] reported that the incorporation of CdS nanoparticles into Dawson-type polyoxometalate (P_2W_{18}) films improved remarkably the photocurrent response and power conversion efficiency. Novais et al. [17] found that

the $\{MG/Co(PW_9)_2\}_n$ multilayer films exhibited excellent electrocatalytic performance for nitrite and iodate reduction with very low detection limits. $(PW_{12}\text{-}TH)_n$ multilayer films deposited on the magnetic substrate of $Fe_3O_4@SiO_2$ microspheres showed a better ability in terms of photocatalytic activity, stability, and reusability than quartz slides [7]. In particular, films can be efficiently separated by a magnet. The Bi_2O_3 nanoparticles assembled into $[SiW_9V_3O_{40}]^{7-}$ endowed the films with specific properties. This film has a tendency toward electrocatalytic L-cysteine and nitrite as well as enhanced electrochromic and photochromic properties [18]. Moreover, the multifunctional films $(PV_6Mo_6/MV)_n$ ($PV_6Mo_6 = (NH_4)_5H_4PV_6Mo_6O_{40}\cdot 6H_2O$, MV = methyl violet) exhibited electrochemical activity for the reduction of NO_2^-, BrO_3^-, and ClO_3^- and remarkable antibacterial properties toward *Escherichia coli*[21]. However, less attention was paid to the photocatalytic performance of $(TiO_2/POM)_n$ composite films coated on $Fe_3O_4@SiO_2$ magnetic microspheres.

In this work, $(TiO_2/POM)_n$ composite films with magnetic and photocatalytic performance were deposited on $Fe_3O_4@SiO_2$ core-shell microspheres by the LbL method. MO was used as the model pollutant to investigate the photocatalytic properties of bifunctional films. The influence of bilayer number deposited on magnetic microspheres, catalyst concentration, inorganic oxidants, and salts on the degradation of the methyl orange solution was studied in detail.

2. Experiments

2.1. Materials. The Fe_3O_4 magnetic microspheres were synthesized following the procedure reported by Sun et al. [22]. Silica-coated magnetic microspheres were prepared through the sol-gel method [7]. Titanium dioxide (TiO_2) colloids were prepared according to literature [23]. $H_3PW_{12}O_{40}\cdot xH_2O$ (PW_{12}), $H_4SiW_{12}O_{40}\cdot xH_2O$ (SiW_{12}), and $H_3PMo_{12}O_{40}\cdot xH_2O$ (PMo_{12}) were obtained from Sinopharm Chemical Reagent Co. Ltd, China. Methyl orange was purchased from Jining Chemical Engineering Research Institute. Commercial polyelectrolytes, poly(sodium 4-styrenesulfonate) (PSS, Mw ~ 70,000) and poly(allylamine hydrochloride) (PAH, Mw ~ 70,000) were obtained from Sigma-Aldrich Inc., USA. Perchloric acid was purchased from Shanghai Jinlu Chemical Co. Ltd, China. Sodium chloride and sodium sulfate were provided by Tianjin Kemiou Chemical Reagent Co. Ltd. Potassium chlorate, potassium bromate, and potassium iodate were obtained from Tianjin Kemiou Chemical Reagent Co. Ltd. Magnesium chloride, aluminium chloride, and sodium hydrogen phosphate were supplied by Aladdin Chemistry Co. Ltd. All reagents were used as received.

2.2. Buildup of $(TiO_2/POM)_n$ Composite Films on Magnetic Microspheres. In order to prepare $(TiO_2/POM)_n$ composite films, 0.2 g $Fe_3O_4@SiO_2$ core-shell microspheres were first immersed in a poly(allylamine hydrochloride) (PAH) and poly(sodium 4-styrenesulfonate) (PSS) aqueous solution for 15 min to gain a surface with uniform charge. Then, the powders were magnetically separated and washed three times with pH 2.0 $HClO_4$ aqueous solution. The concentration of PAH and PSS aqueous solution was fixed as 2.0 g/L containing 0.5 mol/L NaCl. The photocatalytic $(TiO_2/POM)_n$ (POMs = PW_{12}, SiW_{12}, and PMo_{12}; n is the number of TiO_2-PW_{12} bilayers) films on magnetic microspheres were formed by alternative immersion in positively charged TiO_2 (10 g/L, pH ~ 2.0) and negatively charged POM solution (3 mmol/L). The assembly time was limited to 15 min to ensure the saturation adsorption of each component. Rinsing by $HClO_4$ aqueous solution with a pH of 2.0 for three times was conducted after each deposition cycle. The $Fe_3O_4@SiO_2$ microspheres coated with the desired deposition number of TiO_2 and POMs were finally obtained. Then, the obtained catalysts were dried overnight at 60°C before further use. For comparison, $(PSS/TiO_2)_{10}$ and $(PAH/PW_{12})_{10}$ composite films on $Fe_3O_4@SiO_2$ magnetic microspheres were deposited in a similar way.

2.3. Characterization of Magnetic Microspheres. The morphology of magnetic microspheres was monitored using a field emission scanning electron microscope (FESEM, model: JSM-6700F, JEOL, Japan) with an accelerating voltage of 10 kV. The Fourier-transform infrared spectra of the products were recorded on a TR200 spectrometer (Thermo Electron Corporation). The chemical element of magnetic microspheres was detected by energy dispersive X-ray spectroscopy (EDX, model: Oxford X-Max 51-XMX1004, Oxford Instruments Co. Ltd., England). The magnetic property was measured on a MPMS (SQUID)-XL (Quantum Design) vibrating sample magnetometer at 300 K.

2.4. Evaluation of Photocatalytic Activity. The XPA-system photochemical reactor purchased from Xujiang Electromechanical Plant was used to conduct photocatalytic experiments. The photoreactor was equipped with a 300 W medium-pressure mercury lamp with a main emission wavelength of 365 nm. The lamp was horizontally arranged and surrounded by a quartz jacket in which cooling water was circulated to avoid overheating. There was a 20 cm distance between the light source and dye solution. A given amount of catalysts and 50 mL of methyl orange solution were placed in a 100 mL glass beaker thermostated using a water jacket. The temperature of the dye solution was controlled at 28 ± 1°C by adjusting the flow of cooling water. The reaction was performed at MO initial concentrations of 10 mg/L with the pH value of the solution at about 2.0 adjusted by $HClO_4$. In the experiments, the catalyst concentration was fixed at 2 g/L except for a few runs to evaluate the effects of the catalyst concentration and inorganic oxidants. In order to establish the adsorption-desorption equilibrium between the MO molecule and the catalysts' surface, the suspension was ultrasonically dispersed for 30 min in the dark. The photocatalytic decontamination of MO started after the mercury lamp became stable. At given intervals, a certain amount of the reaction solution was taken out and separated. The residual dyes were analyzed by a Shimadzu UV-2450 UV-vis spectrophotometer. The removal rate can be estimated by the following formula:

$$\text{Removal rate}\,(\%) = \frac{A_0 - A}{A_0} \times 100, \quad (1)$$

where A_0 is the original absorbance of the MO solution at the maximum absorption wavelength ($\lambda_{max} = 507$ nm), and A is the residual absorbance of MO after UV-light irradiation.

3. Results and Discussion

3.1. Characterization of Magnetic Microspheres. The surface morphology of magnetic microspheres was examined by FESEM. It is clearly visible from Figure 1 that the Fe_3O_4 microspheres modified by the hydrolyzation of tetraethyl orthosilicate exhibit a typical spherical form, and the average particle sizes are determined to be 150–200 nm. The shape of the magnetic microspheres has no prominent change when TiO_2 colloidal nanoparticles and PW_{12} nanoclusters assembled alternately on the outer surface of Fe_3O_4@SiO_2 microspheres. It also shows that magnetic microspheres are aggregated to a certain extent because of the magnetic dipolar interaction among the particles. Moreover, the composition of magnetic photocatalysts was also confirmed by EDX spectroscopy (Figure 1(c)). EDX analysis reveals the presence of Ti, O, W, P, and Fe on the surfaces of Fe_3O_4@SiO_2 magnetic microspheres. This proves the successful assembly of TiO_2 nanoparticles and polyoxometalate (POM) anions on the surface of Fe_3O_4@SiO_2 microspheres. Meanwhile, a dramatic Pt peak can be seen. Pt comes from the plated platinum used to increase the conductivity of sample.

The assembly process of magnetic microspheres was monitored by FT-IR spectra. The results are shown in Figure 2. The band that appeared at 584 cm^{-1} is assigned to the vibration of the Fe-O bond for Fe_3O_4 particles. After coating a SiO_2 shell by the sol-gel method, three obvious bands at 1100 cm^{-1}, 798 cm^{-1}, and 469 cm^{-1} are assigned to the symmetric and antisymmetric stretching vibration of the Si-O bond. After an alternative deposition of TiO_2 and PW_{12} multilayer films through the LbL method, the intensity of the Fe-O and Si-O bands decreases. This phenomenon is ascribed to the effective screening of TiO_2 and PW_{12} multilayer films on Fe-O and Si-O bands. Meanwhile, the new bands at 960 cm^{-1}, 895 cm^{-1}, and 804 cm^{-1} appear, which associate with typical Keggin skeletal vibration bands for PW_{12}. This is consistent with the previous report [14]. However, the stretching vibration of the P-O bond at 1080 cm^{-1} is covered by a strong peak of the Si-O bond. The FT-IR spectrum of Fe_3O_4@SiO_2@$(TiO_2/PW_{12})_{10}$ microspheres indicates that the Keggin structure of PW_{12} still remains intact.

Figure 3(a) shows the magnetization of Fe_3O_4, Fe_3O_4@SiO_2, and Fe_3O_4@SiO_2@$(TiO_2/PW_{12})_{10}$ microspheres as a function of an applied magnetic field, which was measured by a vibrating sample magnetometer at 300 K. The samples all exhibit a superparamagnetic characteristic. The magnetizations of samples increase with the increase of the applied magnetic field and nearly reach saturation with saturation magnetization (Ms) values of 48.5, 15.8, and 6.0 emu/g, respectively. Compared to Fe_3O_4@SiO_2 microspheres, the Ms values of composite photocatalysts slightly decrease. This is ascribed to the deposition of $(TiO_2/PW_{12})_{10}$ on core-shell Fe_3O_4@SiO_2. Figure 3(b) illustrates the magnetic separation of Fe_3O_4@SiO_2@$(TiO_2/PW_{12})_{10}$ microspheres from the aqueous suspension. The photocatalysts possess a strong magnetic response under an external magnetic field due to the existence of an Fe_3O_4 core. They can be easily removed from the MO solution after photodegradation by an external magnet. Then, a nearly colorless solution is obtained (see Figure 3(b)). The strong magnetic response of photocatalysts ensures their convenient, fast, and efficient separation from the reaction media for reuse.

3.2. Photocatalytic Activity of Magnetic Microspheres. In the photocatalytic procedure, methyl orange (MO) was used as the model organic molecule to evaluate the photocatalytic activity of composite films assembled on Fe_3O_4@SiO_2 magnetic microspheres. The photocatalytic activity of samples toward azo dye MO is shown in Figure 4. In the dark, the degradation of MO is hardly observed even though magnetic films are presented. Only 13.30% of MO can be degraded by direct photolysis after UV-light irradiation for 100 min. After being exposed at the same time, the removal rates of MO in the presence of $(TiO_2/PW_{12})_{10}$, $(TiO_2/PSS)_{10}$, and $(PAH/PW_{12})_{10}$ composite films deposited on Fe_3O_4@SiO_2 microspheres are 83.91%, 28.66%, and 16.44%, respectively. The fast disappearance of MO in the presence of the Fe_3O_4@SiO_2@$(TiO_2/PW_{12})_{10}$ photocatalyst owes to the synergistic effect of TiO_2 and PW_{12}. Since photogenerated electrons can be transferred from the TiO_2 conduction band to the empty orbit of tungstophosphate acid, quantum efficiency can be improved. Accordingly, reactive oxygen species (ROSs) are easy to generate through the reaction of electrons and holes with hydroxyl ion, adsorbed water, and oxygen. These ROSs and active holes are without selectivity and can completely oxidize a MO molecule to CO_2, H_2O, and inorganic salts. However, without the synergistic effect, the fast recombination of photoinduced holes and electrons cannot be avoided in pure TiO_2 or PW_{12} films, which leads to the decrease in photocatalytic efficiency.

Moreover, the photocatalytic efficiency of Fe_3O_4@SiO_2@$(TiO_2/SiW_{12})_{10}$ and Fe_3O_4@SiO_2@$(TiO_2/PMo_{12})_{10}$ magnetic films was also examined for comparison with Fe_3O_4@SiO_2@$(TiO_2/PW_{12})_{10}$. Under the same experimental conditions, the photodegradation of MO by the abovementioned films reaches 62.07% and 13.55%, respectively. These results shown in Figure 5 indicate that $(TiO_2/PW_{12})_{10}$ and $(TiO_2/SiW_{12})_{10}$ composite films deposited on Fe_3O_4@SiO_2 can lead to effective degradation of MO. In particular, a higher efficiency can be obtained from $(TiO_2/PW_{12})_{10}$ films. However, the photocatalytic activity of Fe_3O_4@SiO_2@$(TiO_2/PMo_{12})_{10}$ magnetic microspheres is very low. This is because the reoxidization of reduced PMo_{12} is very difficult.

The effect of (TiO_2/PW_{12}) bilayer number coated on magnetic microspheres on MO decoloration was also investigated. As shown in Figure 6, the removal rate is increased significantly by increasing the $(TiO_2/PW_{12})_n$ bilayer number. After UV-light irradiation for 100 min, the degradation efficiency of MO with 2, 4, 6, 8, and 10 bilayers is 30.46%, 41.14%, 69.75%, 78.79%, and 83.91%, respectively. The highest degradation rate is obtained when the bilayer number of $(TiO_2/PW_{12})_n$ grows to 10. This study reveals that the photocatalytic activity strongly depends on the bilayer number of $(TiO_2/PW_{12})_n$ films. The increase of photocatalytic efficiency

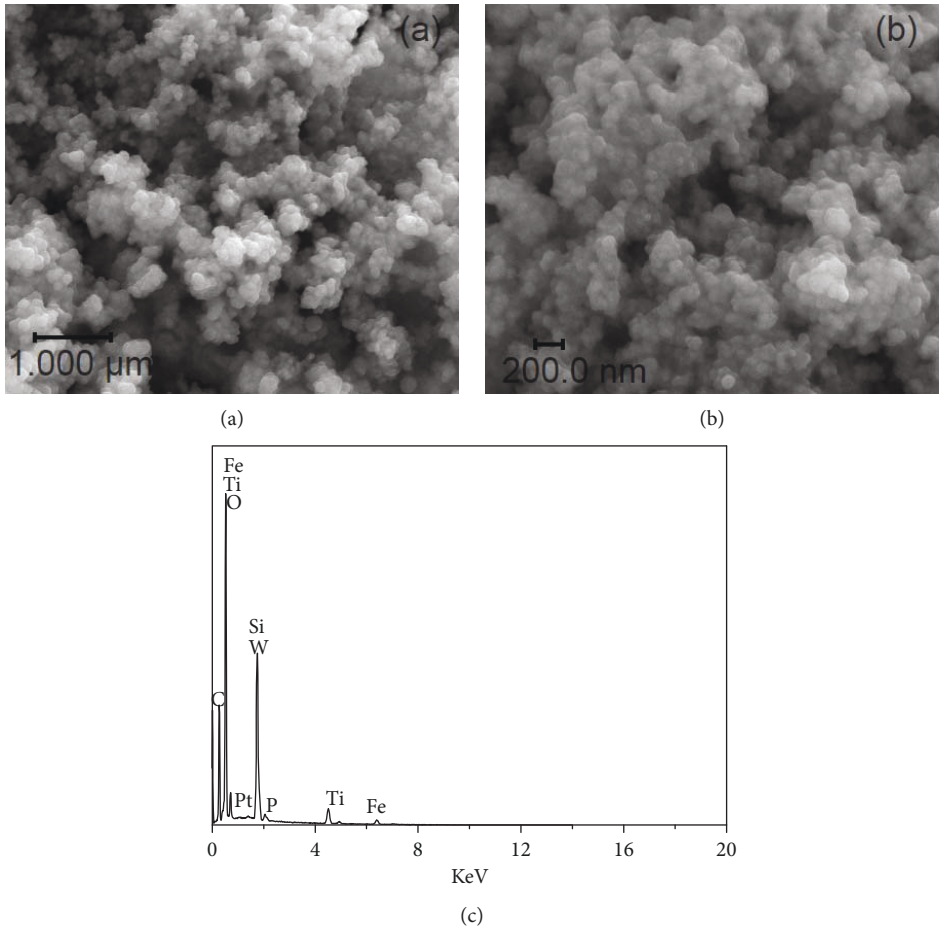

Figure 1: FESEM image of (a) $Fe_3O_4@SiO_2$ core-shell microspheres and (b) $Fe_3O_4@SiO_2@(TiO_2/PW_{12})_{10}$ microspheres. (c) EDX spectrum of $Fe_3O_4@SiO_2$ microspheres coated with a $(TiO_2/PW_{12})_{10}$ film.

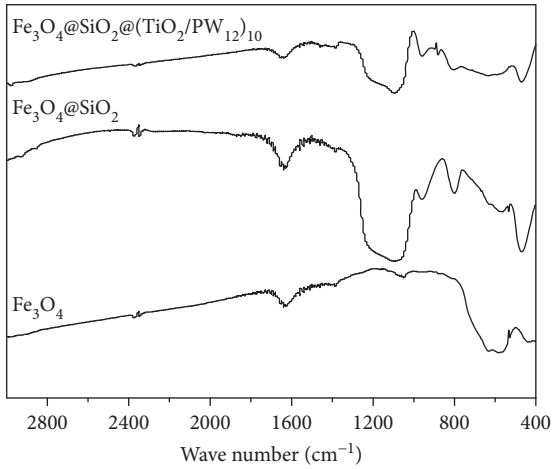

Figure 2: FT-IR spectra of Fe_3O_4 particles, $Fe_3O_4@SiO_2$ microspheres, and $Fe_3O_4@SiO_2@(TiO_2/PW_{12})_{10}$ microspheres.

is attributed to more TiO_2 and PW_{12} nanoparticles effectively deposited on $Fe_3O_4@SiO_2$ core-shell microspheres. It should be noted that $Fe_3O_4@SiO_2$ microspheres have no photocatalytic activity. Thus, the reason why $(TiO_2/PW_{12})_{10}$ magnetic microspheres have a higher photocatalytic efficiency is that the contents of TiO_2 and PW_{12} in $(TiO_2/PW_{12})_{10}$ are higher than in other catalysts.

Figure 7 compares the photodegradation of MO under various concentrations of $Fe_3O_4@SiO_2$ microspheres coated with $(TiO_2/PW_{12})_{10}$ films. The catalyst concentration was selected as 0.2, 0.4, 0.8, 1.4, and 2.0 g/L. It is observed that the degradation rate increases gradually with the growth of the catalyst concentration. In the presence of $(TiO_2/PW_{12})_{10}$ magnetic microspheres, the degradation efficiency of MO with 0.2 g/L of the catalyst is 69.37% after UV-light irradiation for 100 min. When the concentration of the catalyst is 2.0 g/L, $(TiO_2/PW_{12})_{10}$ magnetic microspheres exhibit the excellent degradation capability for MO and around 83.91% of MO molecules are removed. The inset shows the plot of the rate constant (k) versus a sample concentration. It is indicated that the photocatalytic efficiency increased with the catalyst concentration and the optimal concentration was 2.0 g/L. The enhancement of photocatalytic efficiency is mainly relevant to the increase of catalyst concentration, which generates massive active sites. Thus, high efficiency can be obtained when more catalysts are added.

The photocatalytic efficiency of MO by $(TiO_2/PW_{12})_{10}$ films coated on $Fe_3O_4@SiO_2$ microspheres was enhanced when halate was introduced. The comparative results with

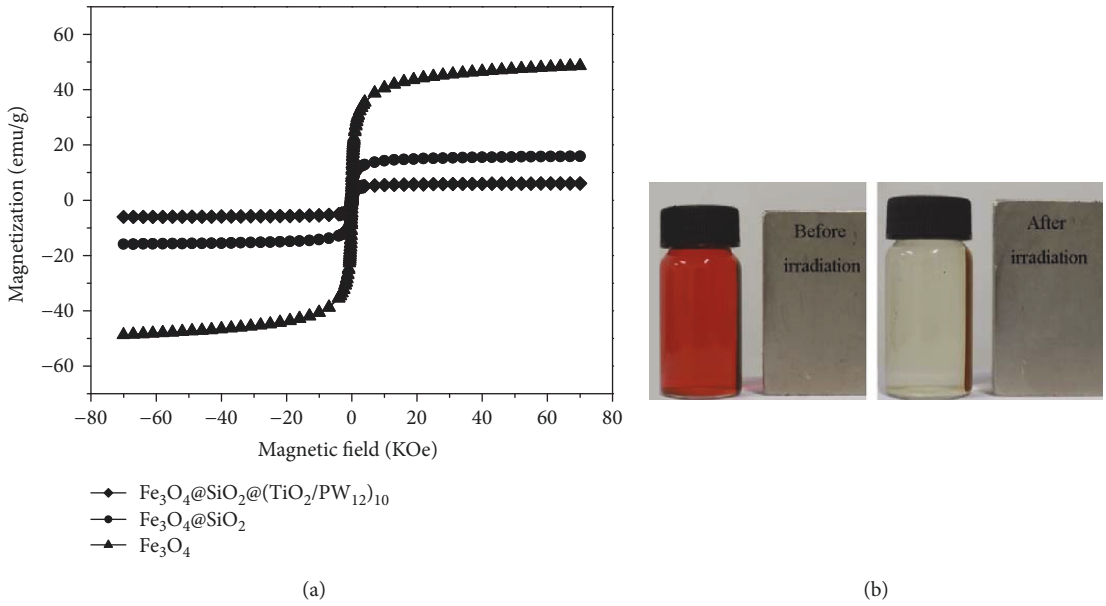

Figure 3: (a) The magnetic hysteresis loops of different samples. (b) Photograph of photocatalysts collected by an external magnet.

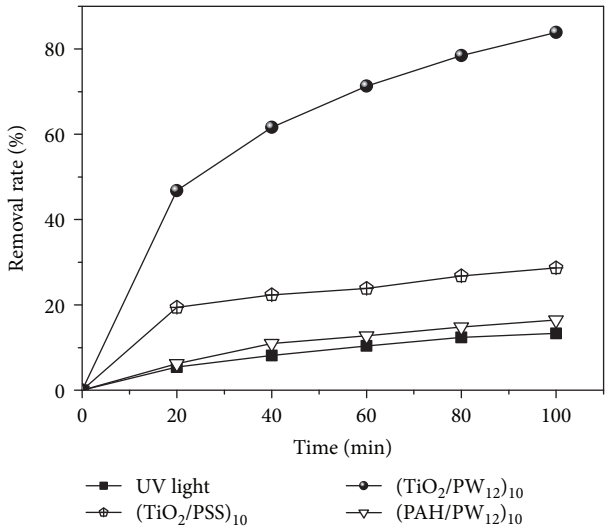

Figure 4: The photocatalytic degradation of methyl orange by different catalysts deposited on $Fe_3O_4@SiO_2$.

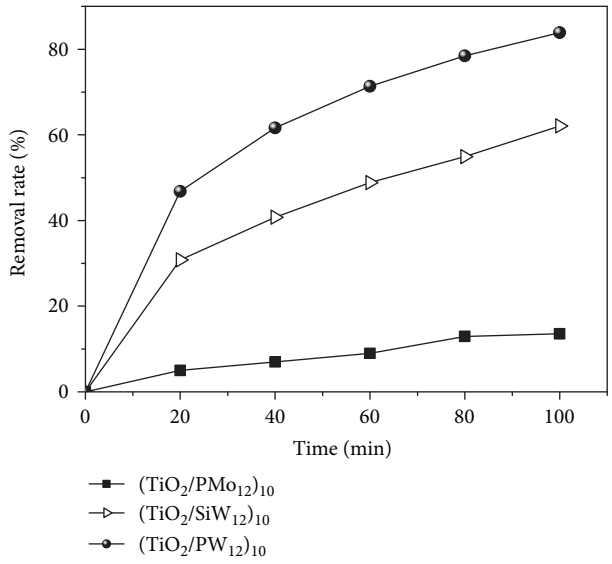

Figure 5: Effect of POM type on MO removal by $Fe_3O_4@SiO_2$ microspheres coated with $(TiO_2/POM)_{10}$ films.

different halate concentrations are shown in Figure 8. It displays a highly positive role in MO degradation due to the addition of halate. The highest degradation rate of 97.32% is obtained at 1 mM BrO_3^- after 40 min of irradiation. Without BrO_3^-, only 52.51% of the MO removal rate is attained within the same amount of time. The enhanced removal rate by the addition of KIO_3, $KBrO_3$, and $KClO_3$ may be attributed to the fact that all of them can act as electron acceptors in the aqueous solution, thus inhibiting electron-hole recombination on the catalysts' surface. The efficiency of BrO_3^- is always higher than that of IO_3^- and ClO_3^-. This is probably related to the higher redox potential of BrO_3^-, which easily reacts with the conduction band electron [24]. The degradation by IO_3^- is accelerated straightforward by the extra radicals such as IO_2• and HIO_3^-•. However, the effect of I^- as the end product of reduction should not be overlooked. The accumulated I^- can result in a significant deterioration of the MO degradation rate [25].

To determine the effect of inorganic salts which always coexists with dye wastewater on the degradation process, different experiments were carried out. Figure 9 shows the results when inorganic salts such as NaCl, $MgCl_2$, $AlCl_3$, Na_2SO_4, and Na_2HPO_4 were added. These salts play different roles in the process of MO photocatalytic degradation. The results shown in Figure 9 reveal that metal chloride has a significant accelerating effect on MO degradation. $AlCl_3$ illustrates the highest photocatalytic efficiency, and the removal

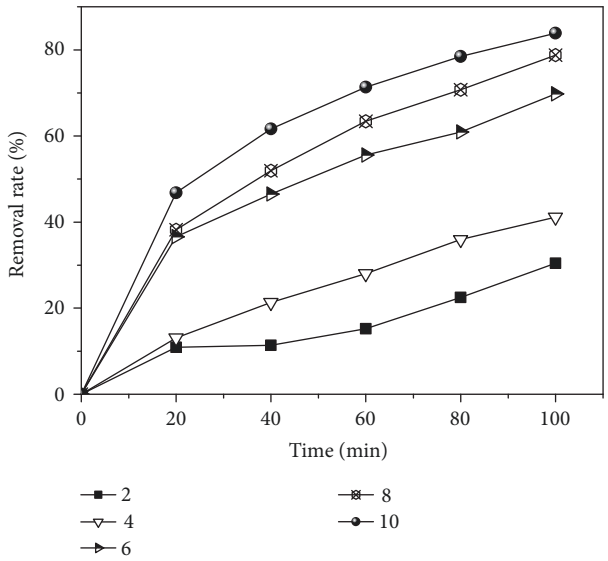

Figure 6: The effect of $(TiO_2/PW_{12})_n$ bilayer number deposited on $Fe_3O_4@SiO_2$ microspheres on MO degradation.

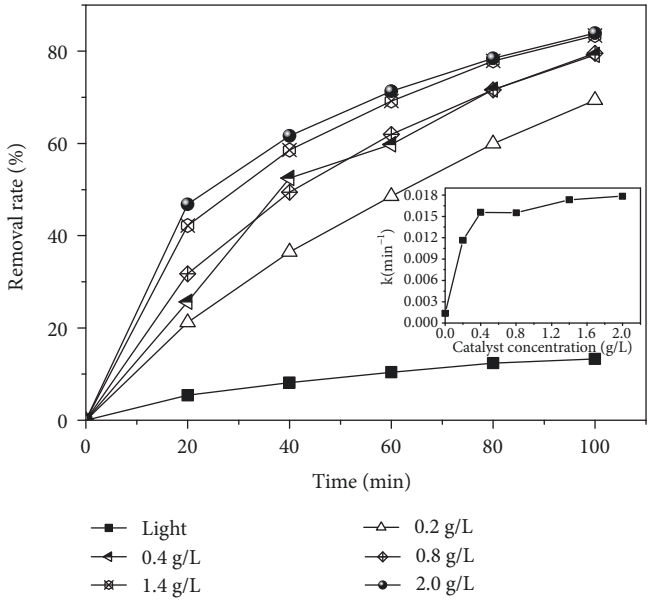

Figure 7: Effect of catalyst concentration on MO degradation by $Fe_3O_4@SiO_2@(TiO_2/PW_{12})_{10}$ magnetic microspheres.

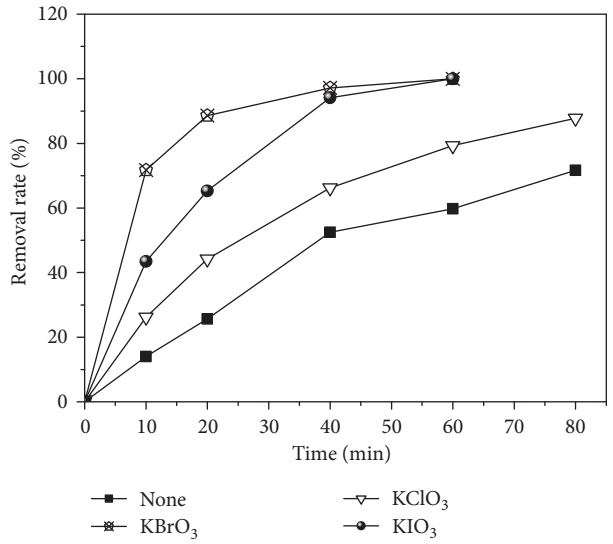

Figure 8: Effect of $KClO_3$, $KBrO_3$, and KIO_3 (1 mM) on MO degradation by $(TiO_2/PW_{12})_{10}$ films coated on $Fe_3O_4@SiO_2$ microspheres (catalyst concentration: 0.4 g/L).

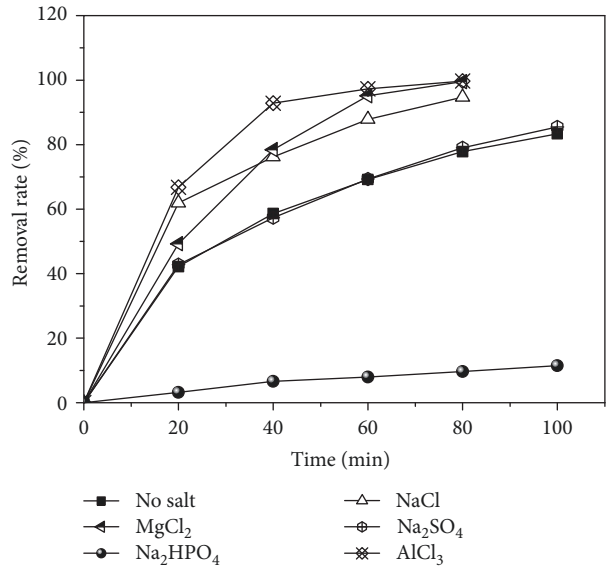

Figure 9: Removal efficiency of MO at different inorganic salts by $Fe_3O_4@SiO_2@(TiO_2/PW_{12})_{10}$ films.

rate reaches 97.32% after being irradiated for 60 min. Na_2SO_4 has no obvious impact on MO removal. However, the addition of Na_2HPO_4 results in a great decrease in the MO degradation rate, which is less than 11.45% after UV-light irradiation for 100 min. The presence of Cl^- ions which leads to the reduction of photocatalytic efficiency has been stated by many previous reports [26–29]. The photocatalytic activity inhibits by Cl^- anion mainly attributed to competitive adsorption between Cl^- and pollutant. However, the positive effect of chloride was achieved in our experiments. This enhancement should be attributed to the efficient formation of chlorine and dichloride anion radicals by scavenging holes and •OH. This process promotes the separation of photogenerated electron-hole pairs [26]. In addition, the higher efficiency of $AlCl_3$ may be related to the charge density δ of the metal cation calculated through the ionic radii. The higher charge density of the metal cation favors the photocatalytic degradation of MO by inhibiting recombination of the intermolecular relaxation of dye molecules with electrons [30]. The decrease of the removal rate by Na_2HPO_4 is due to the addition of Na_2HPO_4 which results in a pH increase of the MO solution. At high pH, $H_3PW_{12}O_{40}$ will be decomposed [15].

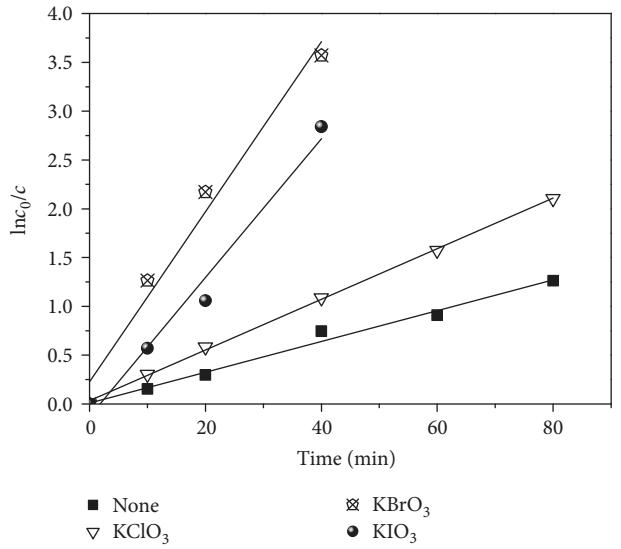

Figure 10: Reaction kinetic study of MO photodegradation under $KClO_3$, $KBrO_3$, and KIO_3.

The reaction kinetics of MO photodegradation in the presence of halate by $Fe_3O_4@SiO_2@(TiO_2/PW_{12})_{10}$ films were investigated. It can be found in Figure 10 that the plots of $\ln c_0/c$ (where c_0 stands for the initial concentration and c is the residual concentration at time t) versus the reaction time yields straight lines. It indicates that the photodecomposition of the diluted MO solution follows apparent first-order kinetics. The first-order rate constants (k) shown in Table 1 were determined from the regression curves of $\ln c_0/c$ versus the reaction time. The constants are $0.01578\,min^{-1}$ without halate, $0.02592\,min^{-1}$ for $KClO_3$, $0.08717\,min^{-1}$ for $KBrO_3$, and $0.07117\,min^{-1}$ for KIO_3. The rate constant increases along with the addition of halate, and the greatest rate constant reaches by 1 mM BrO_3^-. It also confirms that photocatalytic efficiency is enhanced, which ascribes to the effective reception of photogeneration electrons.

4. Conclusions

Photocatalytic $(TiO_2/POM)_n$ film coated on magnetic $Fe_3O_4@SiO_2$ microspheres were prepared based on the electrostatic LbL method. Degradation of methyl orange under UV irradiation was investigated to compare their photocatalytic activity. The presence of PW_{12} and SiW_{12} leads to the effective degradation of MO due to the synergistic effect by combining POMs with TiO_2. However, the reoxidization of reduced PMo_{12} is very difficult, which causes the decline of the catalysts' effectiveness. The degradation of methyl orange is significantly enhanced by increasing the bilayer number and catalyst concentration. The combination with inorganic oxidants enhances significantly the photodecoloration rate of the dye. It is found that 97.32% of MO is removed after 40 min of irradiation by the addition of $KBrO_3$. Analyses on the primary role of inorganic salts demonstrate that the photocatalytic efficiency increases drastically by metal chloride, but strongly decreases by Na_2HPO_4. The degradation reactions of MO follow pseudo first-order kinetics. It is found that the use of magnetic support guarantees a photocatalyst with facile, clean, fast, and efficient separation.

Table 1: The rate constants (k) and linear correlation coefficients (R^2) for MO degradation in the presence of halate.

Halate	k/min^{-1}	R^2
None	0.01578	0.9852
$KClO_3$	0.02592	0.9989
$KBrO_3$	0.08717	0.9691
KIO_3	0.07117	0.9709

Data Availability

The data used to support the findings of this study are available from the corresponding author upon request.

Conflicts of Interest

The authors declare that they have no conflicts of interest.

Acknowledgments

This work was financially supported by the National Natural Science Foundation of Shandong Province Combination Research Projects (ZR2013BL001, ZR2015BL032, and ZR2014BL001).

References

[1] J. Deng, S. F. Feng, X. Y. Ma et al., "Heterogeneous degradation of Orange II with peroxymonosulfate activated by ordered mesoporous $MnFe_2O_4$," *Separation and Purification Technology*, vol. 167, pp. 181–189, 2016.

[2] A. R. Khataee and M. B. Kasiri, "Photocatalytic degradation of organic dyes in the presence of nanostructured titanium dioxide: influence of the chemical structure of dyes," *Journal of Molecular Catalysis A: Chemical*, vol. 328, no. 1-2, pp. 8–26, 2010.

[3] P. A. K. Reddy, P. V. L. Reddy, E. Kwon, K. H. Kim, T. Akter, and S. Kalagar, "Recent advances in photocatalytic treatment of pollutants in aqueous media," *Environment International*, vol. 91, pp. 94–103, 2016.

[4] A. Mylonas and E. Papaconstantinou, "On the mechanism of photocatalytic degradation of chlorinated phenols to CO_2 and HCl by polyoxometalates," *Journal of Photochemistry and Photobiology A: Chemistry*, vol. 94, no. 1, pp. 77–82, 1996.

[5] A. Hiskia, A. Mylonas, and E. Papaconstantinou, "Comparison of the photoredox properties of polyoxometallates and semiconducting particles," *Chemical Society Reviews*, vol. 30, no. 1, pp. 62–69, 2001.

[6] Z. Yang, S. Y. Gao, H. F. Li, and R. Cao, "Synthesis and visible light photocatalytic properties of polyoxometalate-thionine composite films immobilized on porous TiO_2 microspheres," *Journal of Colloid and Interface Science*, vol. 375, pp. 172–179, 2012.

[7] H. F. Li, S. Y. Gao, M. N. Cao, and R. Cao, "Self-assembly of polyoxometalate-thionine multilayer films on magnetic microspheres as photocatalyst for methyl orange degradation

under visible light irradiation," *Journal of Colloid and Interface Science*, vol. 394, pp. 434–440, 2013.

[8] X. Yang, H. Zhao, J. F. Feng, Y. N. Chen, S. Y. Gao, and R. Cao, "Visible-light-driven selective oxidation of alcohols using a dye-sensitized TiO_2-polyoxometalate catalyst," *Journal of Catalysis*, vol. 351, pp. 59–66, 2017.

[9] L. H. Gao, J. F. Zhang, H. L. Wang, X. Y. Lin, J. M. Qi, and K. Z. Wang, "Effects of elemental composition variations of Keggin polyoxometalates on photocurrent generation of their layer-by-layer self-assembled films with a hemicyanine dye," *Electrochimica Acta*, vol. 166, pp. 215–222, 2015.

[10] L. Zhang, S. B. Li, Z. F. Zhang, L. C. Tan, H. J. Pang, and H. Y. Ma, "Facile fabrication of reduced graphene oxide and Keggin-type polyoxometalates nanocomposite film for high performance electrocatalytic oxidation of nitrite," *Journal of Electroanalytical Chemistry*, vol. 807, pp. 97–103, 2017.

[11] S. Y. Gao, D. M. Pan, and R. Cao, "Layer-by-layer self-assembly polytungstogermanate multilayer films and their photocatalytic properties under sunlight irradiation," *Journal of Colloid and Interface Science*, vol. 358, no. 2, pp. 593–597, 2011.

[12] Z. X. Sun, F. Y. Li, L. Xu, S. P. Liu, M. L. Zhao, and B. B. Xu, "Effects of Dawson-type tungstophosphate on photoelectrochemical responses of cadmium sulfide composite film," *The Journal of Physical Chemistry C*, vol. 116, no. 10, pp. 6420–6426, 2012.

[13] W. Yang, L. H. Gao, and K. Z. Wang, "Photoelectric properties of polyoxometalate-based thin films—recent advances and future perspective," *Polyhedron*, vol. 82, pp. 80–87, 2014.

[14] A. Nakajima, T. Koike, S. Yanagida, T. Isobe, Y. Kameshima, and K. Okada, "Preparation and photocatalytic activity of $[PW_xMo_{12-x}O_{40}]^{3-}/TiO_2$ hybrid film composites," *Applied Catalysis A: General*, vol. 385, no. 1-2, pp. 130–135, 2010.

[15] P. Niu and J. C. Hao, "Efficient degradation of organic dyes by titanium dioxide-silicotungstic acid nanocomposite films: influence of inorganic salts and surfactants," *Colloids and Surfaces A: Physicochemical and Engineering Aspects*, vol. 443, pp. 501–507, 2014.

[16] C. H. Sui, C. Wang, Z. Y. Wang et al., "Different coating on electrospun nanofiber via layer-by-layer self-assembly for their photocatalytic activities," *Colloids and Surfaces A: Physicochemical and Engineering Aspects*, vol. 529, pp. 425–433, 2017.

[17] H. C. Novais, D. M. Fernandes, and C. Freire, "Hybrid methyl green/cobalt-polyoxotungstate nanostructured films: self-assembly, electrochemical and electrocatalytic properties," *Applied Surface Science*, vol. 347, pp. 40–47, 2015.

[18] C. X. Li, K. P, H. Y. M. O'halloran, and S. L. Shi, "Multifunctional multilayer films containing polyoxometalates and bismuth oxide nanoparticles," *The Journal of the Physical Chemistry B*, vol. 113, no. 23, pp. 8043–8048, 2009.

[19] L. Zhang, L. Ning, Z. F. Zhang et al., "Fabrication and electrochemical determination of L-cysteine of a composite film based on V-substituted polyoxometalates and Au@2Ag core-shell nanoparticles," *Sensors and Actuators B: Chemical*, vol. 221, pp. 28–36, 2015.

[20] S. P. Liu and X. S. Qu, "Construction of nanocomposite film of Dawson-type polyoxometalate and TiO_2 nanowires for electrochromic applications," *Applied Surface Science*, vol. 412, pp. 189–195, 2017.

[21] X. Yua, C. Y. Chen, J. Peng et al., "Antibacterial-active multilayer films composed of polyoxometalate and methyl violet: fabrication, characterization and properties," *Thin Solid Films*, vol. 571, pp. 69–74, 2014.

[22] H. W. Sun, J. H. Yu, P. J. Gong, D. M. Xu, C. F. Zhang, and S. D. Yao, "Novel core-shell magnetic nanogels synthesized in an emulsion-free aqueous system under UV irradiation for targeted radiopharmaceutical applications," *Journal of Magnetism and Magnetic Materials*, vol. 294, no. 3, pp. 273–280, 2005.

[23] D. G. Shchukin, J. H. Schattka, M. Antonietti, and R. A. Caruso, "Photocatalytic properties of porous metal oxide networks formed by nanoparticle infiltration in a polymer gel template," *The Journal of Physical Chemistry B*, vol. 107, no. 4, pp. 952–957, 2003.

[24] K. Selvam, M. Muruganandham, I. Muthuvel, and M. Swaminathan, "The influence of inorganic oxidants and metal ions on semiconductor sensitized photodegradation of 4-fluorophenol," *Chemical Engineering Journal*, vol. 128, no. 1, pp. 51–57, 2007.

[25] D. Zhang, Y. Q. Zhang, H. Y. Ma, H. Yan, and Y. B. Song, "Fabrication of a 12-tungstophosphate and cadmium oxide composite film and its properties," *Materials Chemistry and Physics*, vol. 144, no. 3, pp. 369–376, 2014.

[26] D. E. Santiago, J. Araña, O. González-Díaz et al., "Effect of inorganic ions on the photocatalytic treatment of agro-industrial wastewaters containing imazalil," *Applied Catalysis B: Environmental*, vol. 156-157, pp. 284–292, 2014.

[27] Y. C. Dong, J. L. Chen, C. H. Li, and H. X. Zhu, "Decoloration of three azo dyes in water by photocatalysis of Fe (III)-oxalate complexes/H_2O_2 in the presence of inorganic salts," *Dyes and Pigments*, vol. 73, no. 2, pp. 261–268, 2007.

[28] M. Muruganandham and M. Swaminathan, "Photochemical oxidation of reactive azo dye with UV-H_2O_2 process," *Dyes and Pigments*, vol. 62, no. 3, pp. 269–275, 2004.

[29] M. Muthukumar and N. Selvakumar, "Studies on the effect of inorganic salts on decolouration of acid dye effluents by ozonation," *Dyes and Pigments*, vol. 62, no. 3, pp. 221–228, 2004.

[30] M. Makita and A. Harata, "Photocatalytic decolorization of rhodamine B dye as a model of dissolved organic compounds: influence of dissolved inorganic chloride salts in seawater of the Sea of Japan," *Chemical Engineering and Processing: Process Intensification*, vol. 47, no. 5, pp. 859–863, 2008.